Double Molecular Photoswitch Driven by Light and Collisions

James N. Bull,[1] Michael S. Scholz,[1] Eduardo Carrascosa,[1] Gabriel da Silva,[2] and Evan J. Bieske[1,*]
[1]School of Chemistry, University of Melbourne, Parkville, Victoria 3010, Australia
[2]Department of Chemical Engineering, University of Melbourne, Parkville, Victoria 3010, Australia

(Received 21 October 2017; published 1 June 2018)

The shapes of many molecules can be transformed by light or heat. Here we investigate collision- and photon-induced interconversions of *EE*, *EZ*, and *ZZ* isomers of the isolated Congo red (CR) dianion, a double molecular switch containing two —*N*=*N*— azo groups, each of which can have the *E* or *Z* configuration. We find that collisional activation of CR dianions drives a one-way $ZZ \rightarrow EZ \rightarrow EE$ cascade towards the lowest-energy isomer, whereas the absorption of a single photon over the 270–600 nm range can switch either azo group from *E* to *Z* or *Z* to *E*, driving the CR dianion to lower- or higher-energy forms. The experimental results, which are interpreted with the aid of calculated statistical isomerization rates, indicate that photoisomerization of CR in the gas phase involves a passage through conical intersection seams linking the excited and ground state potential energy surfaces rather than through isomerization on the ground state potential energy surface following internal conversion.

DOI: 10.1103/PhysRevLett.120.223002

The structural rearrangement of a molecule following the absorption of light plays a crucial role in natural and technological contexts. For example, photoisomerization of the retinal chromophore in an opsin protein initiates the visual transduction cycle in animals [1], while molecules that change shape in response to the absorption of light serve as core transducers in optogenetics [2] and in optically powered molecular machines [3]. One of the most versatile photoisomerizable linkages is the azo (—*N*=*N*—) group [4], which possesses *E* and *Z* geometric arrangements interconvertible through the absorption of light. Molecules containing azo groups have been deployed for photocontrolling peptide structure and foldamers [5,6], photoswitching lipids and membranes [7], photoactivated molecular logic switches [8,9], photoswitching of the chemical structure on gold surfaces [10], and light-induced phase segregation in liquid crystals [11]. Their appeal stems from efficient photoisomerization proceeding on a subpicosecond timescale (quantum yield > 0.2), which is rapid compared to intramolecular and intermolecular vibrational energy relaxation in condensed phases [4,12–14]. For azo molecules such as azobenzene, theory has established that photoisomerization involves conical intersection seams where the central —*N*=*N*— bond has a geometry intermediate between the *E* and *Z* forms [14]. These conical intersections mediate the passage from the excited state surface to the ground state surface with a transformation of electronic energy to vibrational energy (internal conversion) and a probability for a concomitant change of the azo molecule's *E*/*Z* isomeric form (see Fig. 1).

A crucial step towards extending the application of photoswitchable molecules is the development of systems containing several azo subunits that undergo consecutive geometric transformations [31–33]. For example, as shown in Fig. 1, the Congo red (CR) dianion contains two azo bonds and thus possesses three geometric isomers: *EE*, *EZ*, and *ZZ*. In a solution, CR exists as the *EE* isomer and has a low fluorescence quantum yield ($\approx 10^{-4}$ in H_2O). The rapid deactivation of the excited state in solution has been attributed to the internal conversion to the ground electronic

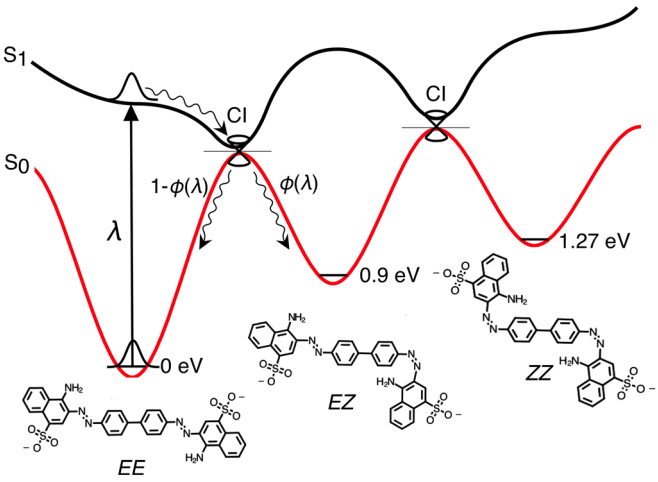

FIG. 1. *EE*, *EZ*, and *ZZ* isomers of the CR dianion with interconversions prompted by light. Relative isomer energies on the S_0 potential energy surface are indicated. S_1/S_0 conical intersections (CIs) associated with isomerization have geometries intermediate between the *E* and *Z* forms. $\phi(\lambda)$ is the photoisomerization quantum yield for wavelength λ. Transition state energies on the S_0 surface were calculated to be 2.13 eV for the *EE* to *EZ* isomerization and 2.38 eV for the *EZ* to *ZZ* isomerization (both values relative to the energy of the *EE* isomer). See Supplemental Material [15] for computational details.

state and the formation of a photoisomer, which reverts back to the most stable *EE* isomer over several hundred picoseconds [34]. Recent gas-phase measurements on CR dianions were also unable to observe fluorescence [35], suggesting a short excited state lifetime. Here we explore the isomerization behavior of the CR dianion in the gas phase, an environment in which complicating interactions with solvent molecules and surfaces are avoided, facilitating direct comparisons between experiment and theory. We demonstrate that, in the gas phase, the three CR isomers survive for longer than 10 ms and can be interconverted using light via pathways that are inaccessible through collisional (thermal) excitation.

We distinguish the *EE*, *EZ*, and *ZZ* CR dianion isomers using ion mobility mass spectrometry, whereby ions are separated according to their collision cross sections as they are propelled through N_2 buffer gas by an electric field [36,37]. Folded, compact ions travel more quickly than unfolded, extended ions. The technique has become a widespread means to characterize the structures of proteins and biomolecules [38] and has recently been applied to follow molecular photoisomerization in the gas phase [39–46]. The tandem ion mobility spectrometer is described in Supplemental Material [15] and Refs. [39,40]. Briefly, CR dianions dissolved in methanol ($\approx 10^{-5}$ mol L^{-1}) were electrosprayed and introduced as packets of ions into the drift region, where they were propelled by an electric field (44 V cm^{-1}) through N_2 buffer gas ($\approx$ 6 Torr), eventually passing through a quadrupole mass filter and striking an ion detector. An arrival time distribution (ATD, the ion signal plotted against the transit time) exhibits peaks corresponding to different isomers.

The ATD of electrosprayed CR dianions [Fig. 2(a)] displays a single peak assigned to the *EE* isomer, the most stable form (see Fig. 1). Exposing the CR solution to 532, 425, or 365 nm light before electrospray ionization had no effect on the ATD, consistent with the rapid thermal reversion of the *EZ* and *ZZ* isomers to the *EE* isomer in a solution [34,47,48]. However, exposing the ions to a 5 ns pulse of 532 nm light immediately after their injection into the drift region of the ion mobility mass spectrometer resulted in the appearance of two additional ATD peaks [Fig. 2(b)], attributable to more compact *EZ* and *ZZ* isomers [49]. The assignment of the three peaks to the *EE*, *EZ*, and *ZZ* isomers is supported by calculated collision cross sections (see Supplemental Material [15]) and also by their photoresponses (see below).

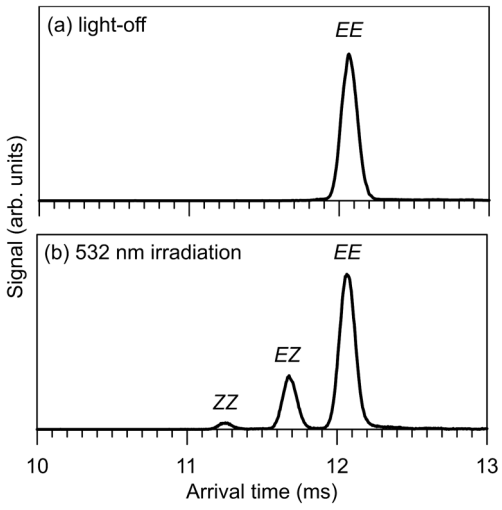

FIG. 2. Arrival time distribution of CR dianions obtained with (a) no light and (b) ions exposed to a pulse of 532 nm light at the start of the drift region.

Photoresponses of *EE*, *EZ*, and *ZZ* isomers were probed by intercepting mobility-selected ions with a second light pulse midway through the drift region [50]. Every second ion packet was irradiated, yielding light-on and light-off ATDs, the difference between which constitutes a photoaction ATD. Light-off and photoaction ATDs for mobility-selected *EE*, *EZ*, and *ZZ* isomers are shown in the upper row in Fig. 3 [51]. Photoisomerization action (PISA) spectra were obtained by plotting the integrated photoisomer signal *S*, normalized by the total light-off ion signal and light pulse energy, against the wavelength (lower row in Fig. 3). These spectra were accumulated with low light pulse energies (< 0.5 mJ cm^{-2} per pulse) whereby a single photon induces isomerization of a single azo bond. Photoaction ATDs recorded at 480 and 350 nm for a range of light pulse energies confirm that the absorption of a single photon causes isomerization about only one of the two azo bonds (see Supplemental Material [15]).

The *EE*, *EZ*, and *ZZ* PISA spectra show two distinct bands [Fig. 3(a)]. For the *EE* isomer, the first band, which peaks at 505 nm, is similar to the corresponding absorption band for CR dissolved in methanol. The second band extends from 270 to 400 nm and has a peak at 370 nm, which is redshifted by $\approx$25 nm relative to the corresponding band for CR in a solution. The visible and UV bands in the PISA spectra of the *EZ* and *ZZ* isomers are both shifted to shorter wavelengths compared to the bands in the *EE* PISA spectrum, presumably due to the disruption of conjugation associated with the loss of planarity. Irradiating the *EZ* isomer produces both the *EE* and *ZZ* isomers [Fig. 3(b)], with a ZZ/EE branching ratio of $\approx$0.8 over the first band, diminishing to ≤ 0.3 over the second band, with some wavelength dependence. The PISA spectrum for the *ZZ* isomer recorded on the *EZ* channel is similar in appearance to the $EZ \rightarrow EE$ spectrum.

The *EE* PISA spectrum agrees with a recent gas-phase multiphoton dissociation spectrum over the 480–600 nm range [35], although the dissociation spectrum exhibits a further peak at $\approx$450 nm whose origin is unknown. The present study implies that the multiphoton dissociation spectrum, which reportedly resulted from three-photon absorption, will be dominated by the *EE* isomer but also have contributions from *EZ* and *ZZ* isomers.

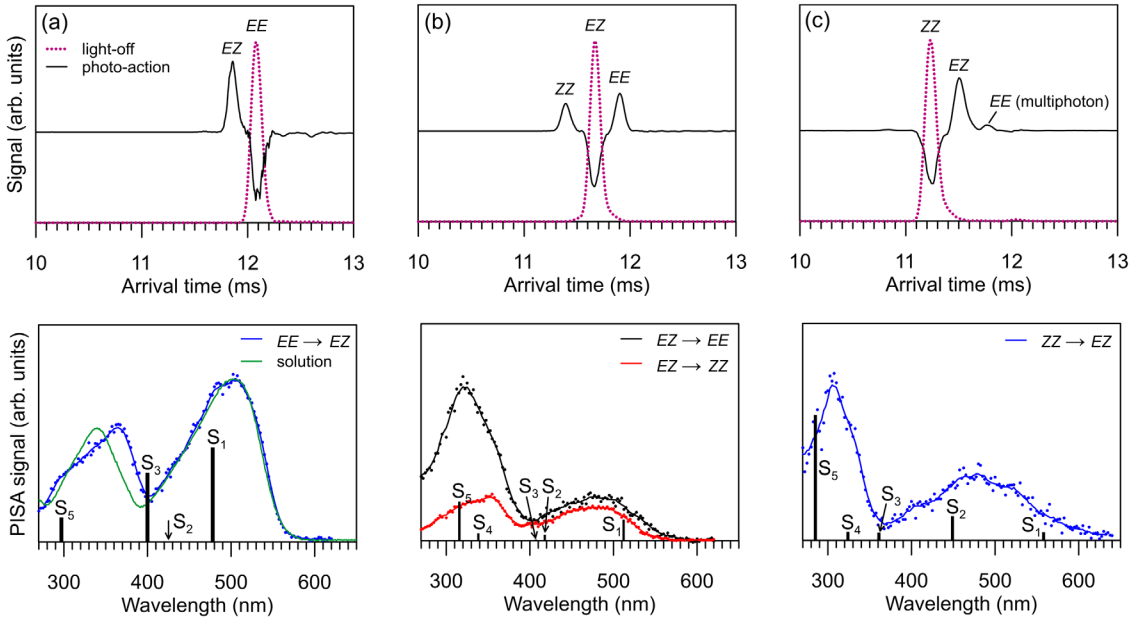

FIG. 3. Photoinduced transformations of (a) *EE*, (b) *EZ*, and (c) *ZZ* isomers of CR. The upper row shows light-off and photoaction ATDs at 480 nm. PISA spectra are shown in the lower row. The absorption spectrum of CR dissolved in methanol is included in (a). Sticks in the PISA plots represent calculated vertical electronic transitions (see Supplemental Material [15]).

We now consider the mechanism for photoisomerization of CR. Following photoexcitation, CR dianions can electronically relax through two mechanisms: (i) Excited molecules undergo rapid isomerization through a conical intersection seam connecting the excited and ground electronic states; (ii) excited molecules internally convert to the ground electronic state, retaining the parent isomer geometry. In both cases, statistical (thermal) isomerization on the ground electronic state potential energy surface may occur before the vibrationally energized isomers are deactivated through buffer gas collisions. Excited CR molecules can also fluoresce, leaving them with insufficient energy to isomerize, although, given that the fluorescence quantum yield for CR in a solution is $\leq 10^{-4}$ [34], this process is unlikely to be significant in the gas phase [35]. Assuming single-photon absorption conditions, the photoisomer signal $S(A \rightarrow B)$ for photoisomer B generated from parent isomer A is proportional to

$$\begin{aligned} S(A \rightarrow B) \approx{}& \sigma_A(\lambda)\phi_{A\rightarrow B}(\lambda) \\ & - \sigma_A(\lambda)\phi_{A\rightarrow B}(\lambda)P_{B\rightarrow X}(E-\Delta) \\ & + \sigma_A(\lambda)[1-\phi_{A\rightarrow B}(\lambda)]P_{A\rightarrow B}(E), \end{aligned} \quad (1)$$

where Δ is the electronic energy difference between isomers A and B, $\sigma_A(\lambda)$ is the absorption cross section of A, $\phi_{A\rightarrow B}(\lambda)$ is the direct photoisomerization quantum yield, and $P_{B\rightarrow X}(E-\Delta)$ and $P_{A\rightarrow B}(E)$ are thermal isomerization probabilities (see Supplemental Material [15]) for total energy $E = E_\lambda + E_T$, where E_λ is the photon energy and E_T is the average thermal energy of the ions at 300 K. The first term, $\sigma_A(\lambda)\phi_{A\rightarrow B}(\lambda)$, corresponds to "prompt" or direct isomerization through a conical intersection connecting the excited state and ground state. The second (negative) term corresponds to "delayed" or secondary thermal isomerization processes on the electronic ground state converting the nascent photoisomer B to other isomer(s) X (which may include A). The third term corresponds to secondary thermal isomerization from vibrationally hot A to B.

The influence of secondary thermal isomerization on the overall isomerization yield was explored through Rice-Ramsperger-Kassel-Marcus (RRKM) and coupled master equation statistical modeling (full details in Supplemental Material [15]). In the first instance, values for the microscopic rate constants $k(E)$ for secondary thermal isomerization were obtained from the RRKM theory using calculated isomer energies and transition states (isomerization barriers) given in Fig. 1. The $k(E)$ values (Table I) assume that the average vibrational energy at 300 K plus the energy imparted through the absorption of a 300, 400, or 500 nm photon becomes statistically distributed among

TABLE I. RRKM microscopic rate coefficients, $k(E)$ with units of s^{-1}, for statistical isomerization assuming a total energy that is the sum of the initial average energy for CR at 300 K plus the energy of a 500, 400, or 300 nm photon.

	500 nm	400 nm	300 nm
$k_{EE\rightarrow EZ}(E)$	9.40×10^{-3}	1.41×10^{-1}	5.46×10^{0}
$k_{EZ\rightarrow EE}(E)$	7.28×10^{3}	4.50×10^{4}	4.98×10^{5}
$k_{EZ\rightarrow ZZ}(E)$	6.53×10^{1}	5.28×10^{2}	8.28×10^{3}
$k_{ZZ\rightarrow EZ}(E)$	1.81×10^{4}	9.53×10^{4}	8.49×10^{5}

all vibrational modes. Because at 6 Torr the collision rate is $\approx 10^9$ s^{-1} and because hundreds of collisions are required to thermalize photoactivated ions [52], energized molecules with $k(E) < 10^7 - 10^8$ s^{-1} are likely to undergo collisional quenching before statistical isomerization.

Consideration of the $k(E)$ values (Table I) indicates that there should be minimal secondary thermal isomerization following the excitation of any of the isomers over the $\lambda = 280$–640 nm range. This implies that the observed photoisomerization signals in Fig. 3 result from excited state dynamics. Provided $\phi(\lambda)$ is independent of λ for each transformation, one would expect that the total PISA spectrum for each isomer should match the corresponding absorption spectrum. Indeed, the band maxima and intensities for the *EE* isomer PISA spectrum are consistent with the calculated wavelengths and oscillator strengths and to the absorption spectrum for CR in solution [Fig. 3(a)].

Photoexcitation of the *EZ* isomer leads to both *EE* and *ZZ* photoisomers [Figs. 2(b) and 3(b)] with near equal production of *EE* and *ZZ* isomers over the visible band but with a preponderance of the *EE* isomer over the UV band. The enhanced yield of the *EE* isomer for the shorter wavelength band could arise because the $S_4 \leftarrow S_0$ and/or $S_5 \leftarrow S_0$ transitions may preferentially lead to the *EE* isomer. In addition, coupled master equation modeling (see Supplemental Material [15]) suggests some minor (<10%) thermal reconversion of *ZZ* photoisomers to the *EZ* form for $\lambda < 350$ nm, consistent with a reduced *ZZ* photoisomer yield. The rate for thermal isomerization of the *EZ* isomer following photoexcitation and recovery of the ground electronic state is predicted to be low ($<10^6$ s^{-1}) over the 280–640 nm range. The rate for reconversion of the *EE* isomer to the *EZ* isomer is predicted to be very low. Last, photoexcitation of the *ZZ* isomer predominately yields the *EZ* photoisomer [Fig. 3(c)]. Secondary thermal $ZZ \rightarrow EZ$ isomerization following the recovery of the ground electronic state is predicted to be slow following the absorption of a visible photon but faster for a UV photon, possibly enhancing the intensity of the shorter wavelength band (< 10% from the coupled master equation modeling in Supplemental Material [15]).

Having established that reversible photoisomerization occurs between *EE*, *EZ*, and *ZZ* isomers, we investigated the effect of collisional excitation by passing the ions through a short 3 mm collision region (slammer) midway through the drift region, in which the electric field could be adjusted from 40 to 550 V cm^{-1} [41,43,53,54]. As shown in Fig. 4, collisions induce a one-way cascade from $ZZ \rightarrow EZ \rightarrow EE$, taking the system to its lowest-energy form. In principle, the threshold slammer voltage for isomerization is related to the isomerization barrier's magnitude [53,54]. However, the present data indicate that, near the threshold, collision-induced isomerization is incomplete in the slammer region. For example, when starting from the *ZZ* isomer, the threshold for $EZ \rightarrow EE$ conversion is ≈90 V, some 15 V higher than the threshold for *EE* formation when the *EZ* isomer is selected. The difference presumably arises because $ZZ \rightarrow EZ$ and $EZ \rightarrow EE$ isomerizations are slow near the threshold and are not completed while the ions are in the slammer region, where the residence time is ≈5 μs at a 100 V slammer potential difference.

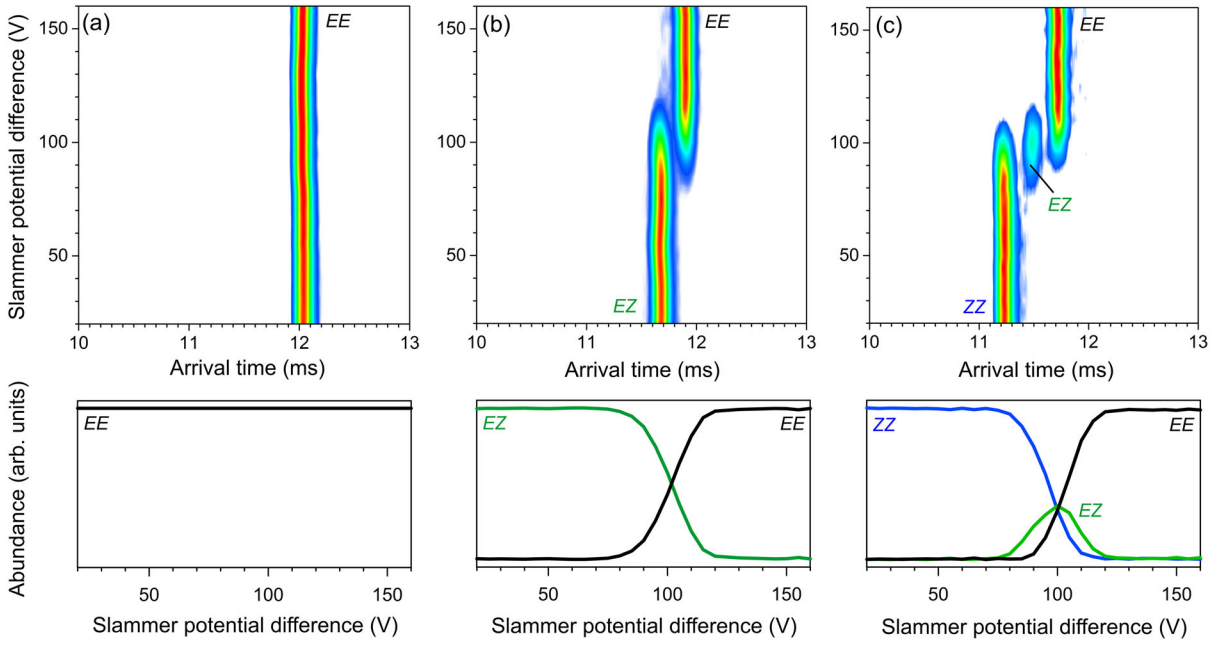

FIG. 4. Transformations of (a) *EE*, (b) *EZ*, and (c) *ZZ* isomers of CR with collisional excitation. The upper row shows ATDs as a function of the slammer potential difference, and the lower row shows the abundance of each isomer with the slammer potential difference.

In summary, the absorption of a visible or near-UV photon drives independent $Z \rightarrow E$ and $E \rightarrow Z$ geometric transformations for the two azo bonds in CR, allowing transformations between EE, EZ, and ZZ forms. In contrast, energetic collisions with buffer gas molecules induce a one-way $ZZ \rightarrow EZ \rightarrow EE$ cascade towards the lowest-energy form. These observations, along with statistical rate calculations, suggest that toggling between the three geometric forms of CR with light relies on excited state dynamics rather than the direct conversion of electronic energy to vibrational energy followed by the statistical crossing of isomerization barriers.

This research was supported under the Australian Research Council's Discovery Project and Future Fellowship funding schemes (Projects No. DP150101427, No. DP160100474, and No. FT130101304). J. N. B. acknowledges resources from the Australian National Computational Infrastructure (NCI) through Early Career Allocation ya1 and a Microsoft Azure Research Award. M. S. S. thanks the Australian government for an Australian Postgraduate Award scholarship. E. C. acknowledges support by the Austrian Science Fund (FWF) through a Schrödinger Fellowship (No. J4013-N36).

*evanjb@unimelb.edu.au

[1] O. P. Ernst, D. T. Lodowski, M. Elstner, P. Hegemann, L. S. Brown, and H. Kandori, Chem. Rev. **114**, 126 (2014).
[2] T. Fehrentz, M. Schönberger, and D. Trauner, Angew. Chem., Int. Ed. **50**, 12156 (2011).
[3] S. Silvi, M. Venturi, and A. Credi, Chem. Commun. (Cambridge) **47**, 2483 (2011).
[4] A. A. Beharry and G. A. Woolley, Chem. Soc. Rev. **40**, 4422 (2011).
[5] C. Renner, U. Kusebauch, M. Löweneck, A. G. Milbradt, and L. Moroder, J. Pept. Res. **65**, 4 (2005).
[6] S. Steinwand, Z. Yu, S. Hecht, and J. Wachtveitl, J. Am. Chem. Soc. **138**, 12997 (2016).
[7] Y. Einaga, T. Yamamoto, T. Sugai, and O. Sato, Chem. Mater. **14**, 4846 (2002).
[8] C. Zhang, M.-H. Du, H.-P. Cheng, X.-G. Zhang, A. E. Roitberg, and J. L. Krause, Phys. Rev. Lett. **92**, 158301 (2004).
[9] Y. Kim, A. Garcia-Lekue, D. Sysoiev, T. Frederiksen, U. Groth, and E. Scheer, Phys. Rev. Lett. **109**, 226801 (2012).
[10] M. J. Comstock, N. Levy, A. Kirakosian, J. Cho, F. Lauterwasser, J. H. Harvey, D. A. Strubbe, J. M. J. Frećhet, D. Trauner, S. G. Louie, and M. F. Crommie, Phys. Rev. Lett. **99**, 038301 (2007).
[11] B. Zupančič, S. Diez-Berart, D. Finotello, O. D. Lavrentovich, and B. Zalar, Phys. Rev. Lett. **108**, 257801 (2012).
[12] T. Schultz, J. Quenneville, B. Levine, A. Toniolo, T. J. Martínez, S. Lochbrunner, M. Schmitt, J. P. Shaffer, M. Z. Zgierski, and A. Stolow, J. Am. Chem. Soc. **125**, 8098 (2003).
[13] J. Bao and P. M. Weber, J. Am. Chem. Soc. **133**, 4164 (2011).
[14] H. M. D. Bandara and S. C. Burdette, Chem. Soc. Rev. **41**, 1809 (2012).
[15] See Supplemental Material at http://link.aps.org/supplemental/10.1103/PhysRevLett.120.223002 for experimental methods, computational methods and results, isomerization yields with light pulse fluence, and master equation modeling of secondary thermal isomerization, which includes Refs. [16–30].
[16] M. W. Schmidt, K. K. Baldridge, J. A. Boatz, S. T. Elbert, M. S. Gordon, J. H. Jensen, S. Koseki, N. Matsunaga, K. A. Nguyen, S. Su, T. L. Windus, M. Dupuis, and J. A. Montgomery, Jr., J. Comput. Chem. **14**, 1347 (1993).
[17] F. Neese, Comput. Mol. Sci. **2**, 73 (2012).
[18] A. D. Becke, J. Chem. Phys. **98**, 1372 (1993).
[19] C. Riplinger, B. Sandhoefer, A. Hansen, and F. Neese, J. Chem. Phys. **139**, 134101 (2013).
[20] T. H. Dunning, Jr., J. Chem. Phys. **90**, 1007 (1989).
[21] N. Minezawa and M. S. Gordon, J. Phys. Chem. A **113**, 12749 (2009).
[22] I. Campuzano, M. F. Bush, C. V. Robinson, C. Beaumont, K. Richardson, H. Kim, and H. I. Kim, Anal. Chem. **84**, 1026 (2012).
[23] M. F. Mesleh, J. M. Hunter, A. A. Shvartsburg, G. C. Schatz, and M. F. Jarrold, J. Phys. Chem. **100**, 16082 (1996).
[24] B. H. Besler, K. M. Merz, Jr., and P. A. Kollman, J. Comput. Chem. **11**, 431 (1990).
[25] M. Quick, A. L. Dobryakov, M. Gerecke, C. Richter, F. Brendt, I. N. Ioffe, A. A. Granovsky, R. Mahrwald, N. P. Ernsting, and S. A. Kovalenko, J. Phys. Chem. B **118**, 8756 (2014).
[26] J. Casellas, M. J. Bearpark, and M. Reguero, ChemPhysChem **17**, 3068 (2016).
[27] J. R. Barker, Int. J. Chem. Kinet. **33**, 232 (2001).
[28] J. R. Barker, Int. J. Chem. Kinet. **41**, 748 (2009).
[29] J. R. Barker, T. L. Nguyen, J. F. Stanton, C. Aieta, M. Ceotto, F. Gabas, T. J. D. Kumar, C. G. L. Li, L. L. Lohr, A. Maranzana, N. F. Ortiz, J. M. Preses, J. M. Simmie, J. A. Sonk, and P. J. Stimac, Multiwell-2017 software suite, University of Michigan, Ann Arbor, MI, 2017, http://clasp-research.engin.umich.edu/multiwell/.
[30] A. K. Y. Lam, C. Li, G. Khairallah, B. B. Kirk, S. J. Blanksby, A. J. Trevitt, U. Wille, R. A. J. O'Hair, and G. da Silva, Phys. Chem. Chem. Phys. **14**, 2417 (2012).
[31] D. Bléger, J. Dokić, M. V. Peters, L. Grubert, P. Saalfrank, and S. Hecht, J. Phys. Chem. B **115**, 9930 (2011).
[32] L. Liu and P. R. Onck, Phys. Rev. Lett. **119**, 057801 (2017).
[33] F. Zhao, L. Grubert, S. Hecht, and D. Bléger, Chem. Commun. (Cambridge) **53**, 3323 (2017).
[34] A. L. Costa, A. C. Gomes, M. Pillinger, I. S. Gonçalves, J. Pina, and J. S. Seixas de Melo, ChemPhysChem **18**, 564 (2017).
[35] C. Kjær, J. M. Lisy, and S. Brønsted Neilsen, J. Phys. Chem. A **122**, 3211 (2018).
[36] G. A. Eiceman, Z. Karpas, and H. H. Hill, *Ion Mobility Spectrometry*, 3rd ed. (CRC Press, Boca Raton, FL, 2013).
[37] M. Vonderach, O. T. Ehrler, P. Weis, and M. M. Kappes, Anal. Chem. **83**, 1108 (2011).
[38] F. Lanucara, S. W. Holman, C. J. Gray, and C. E. Eyers, Nat. Chem. **6**, 281 (2014).

[39] B. D. Adamson, N. J. A. Coughlan, R. E. Continetti, and E. J. Bieske, Phys. Chem. Chem. Phys. **15**, 9540 (2013).
[40] B. D. Adamson, N. J. A. Coughlan, P. B. Markworth, R. E. Continetti, and E. J. Bieske, Rev. Sci. Instrum. **85**, 123109 (2014).
[41] N. J. A. Coughlan, M. S. Scholz, C. S. Hansen, A. J. Trevitt, B. D. Adamson, and E. J. Bieske, J. Am. Soc. Mass Spectrom. **27**, 1483 (2016).
[42] P. B. Markworth, B. D. Adamson, N. J. A. Coughlan, L. Goerigk, and E. J. Bieske, Phys. Chem. Chem. Phys. **17**, 25676 (2015).
[43] J. N. Bull, M. S. Scholz, N. J. A. Coughlan, and E. J. Bieske, Phys. Chem. Chem. Phys. **19**, 12776 (2017).
[44] J. N. Bull, E. Carrascosa, N. Mallo, M. S. Scholz, G. da Silva, J. E. Beves, and E. J. Bieske, J. Phys. Chem. Lett. **9**, 665 (2018).
[45] J. N. Bull, N. J. A. Coughlan, and E. J. Bieske, J. Phys. Chem. A **121**, 6021 (2017).
[46] I. Czerwinska, A. Kulesza, C. Choi, F. Chirot, A.-L. Simon, J. Far, C. Kune, E. De Pauw, and P. Dugourd, Phys. Chem. Chem. Phys. **18**, 32331 (2016).
[47] J. N. Bull, M. S. Scholz, N. J. A. Coughlan, A. Kawai, and E. J. Bieske, Anal. Chem. **88**, 11978 (2016).
[48] J. N. Bull, E. Carrascosa, M. S. Scholz, N. J. A. Coughlan, and E. J. Bieske, Analyst **142**, 2100 (2017).
[49] Because the ATD peaks are baseline resolved, thermal reversion must occur on a longer timescale than the drift time (≈12 ms).
[50] An ion gate situated immediately before the photoisomerization or collision region selected ions with a narrow distribution of collision cross sections (typically ≈4 $Å^2$ broad).
[51] In the ATDs, $t = 0$ corresponds to ion injection into the drift region. Because the second light pulse intercepts the ions halfway along the drift region, photoisomer peaks in photoaction ATDs appear between the parent isomer peak and the product isomer peak if it was separated over the entire drift region. Photodepletion of the parent isomer was always matched by formation of photoisomers (see photoaction ATDs in Fig. 3), indicating that photodestruction was negligible. The absence of photodissociation was confirmed by recording photoaction ATDs with the quadrupole mass filter set to transmit all ions. Seeding the buffer gas with 5% SF_6 resulted in only traces of SF_6^-, proving photodetachment was negligible.
[52] G. W. Flynn, C. S. Parmenter, and A. M. Wodtke, J. Phys. Chem. **100**, 12817 (1996).
[53] N. A. Pierson, L. Chen, D. H. Russell, and D. E. Clemmer, J. Am. Chem. Soc. **135**, 3186 (2013).
[54] N. A. Pierson and D. E. Clemmer, Int. J. Mass Spectrom. **377**, 646 (2015).